UNITED NATIONS EDUCATIONAL, SCIENTIFIC AND CULTURAL ORGANIZATION
INTERNATIONAL CENTRE FOR THEORETICAL PHYSICS
I.C.T.P., P.O. BOX 586, 34100 TRIESTE, ITALY, CABLE: CENTRATOM TRIESTE

UNITED NATIONS INDUSTRIAL DEVELOPMENT ORGANIZATION

INTERNATIONAL CENTRE FOR SCIENCE AND HIGH TECHNOLOGY
c/o INTERNATIONAL CENTRE FOR THEORETICAL PHYSICS 34100 TRIESTE (ITALY) VIA GRIGNANO, 9 (ADRIATICO PALACE) P.O. BOX 586 TELEPHONE 040-224572 TELEFAX 040-224575 TELEX 460449 APH I

H4.SMR/676-34

SECOND SCHOOL ON THE USE OF SYNCHROTRON RADIATION IN SCIENCE AND TECHNOLOGY: *"JOHN FUGGLE MEMORIAL"*

25 October - 19 November 1993

Miramare - Trieste, Italy

Single Crystal Crystallography

M. Colapietro
Università degli Studi di Roma "La Sapienza
Rome, Italy

Since the core deformation scattering is negligible ΔF practically coincides with deformation scattering of the valence shells.

Diffraction by a crystal

One three-dimensional infinite lattice can be represented (see Appendix 3.A, p. 174) by the lattice function

$$L(\boldsymbol{r}) = \sum_{u,v,w=-\infty}^{+\infty} \delta(\boldsymbol{r} - \boldsymbol{r}_{u,v,w})$$

where δ is the Dirac delta function and $\boldsymbol{r}_{u,v,w} = u\boldsymbol{a} + v\boldsymbol{b} + w\boldsymbol{c}$ (with u, v, w being integers) is the generic lattice vector. Let us suppose that $\rho_M(\boldsymbol{r})$ describes the electron density in the unit cell of an infinite three-dimensional crystal. The electron density function for the whole crystal (see Appendix 3.A, p. 183) is the convolution of the $L(\boldsymbol{r})$ function with $\rho_M(\boldsymbol{r})$:

$$\rho_\infty(\boldsymbol{r}) = \rho_M(\boldsymbol{r}) * L(\boldsymbol{r}). \tag{3.23}$$

As a consequence of eqns (3.A.35), (3.A.30), and (3.22) the amplitude of the wave scattered by the whole crystal is

$$\begin{aligned} F_\infty(\boldsymbol{r}^*) &= \mathrm{T}[\rho_M(\boldsymbol{r})] \cdot \mathrm{T}[L(\boldsymbol{r})] \\ &= F_M(\boldsymbol{r}^*) \cdot \frac{1}{V} \sum_{h,k,l=-\infty}^{+\infty} \delta(\boldsymbol{r}^* - \boldsymbol{r}^*_{\mathbf{H}}) \\ &= \frac{1}{V} F_M(\mathbf{H}) \sum_{h,k,l=-\infty}^{+\infty} \delta(\boldsymbol{r}^* - \boldsymbol{r}^*_{\mathbf{H}}) \end{aligned} \tag{3.24}$$

where V is the volume of the unit cell and $\boldsymbol{r}^*_{\mathbf{H}} = h\boldsymbol{a}^* + k\boldsymbol{b}^* + l\boldsymbol{c}^*$ is the generic lattice vector of the reciprocal lattice (see pp. 63–5).

If the scatterer object is non-periodic (atom, molecule, etc.) the amplitude of the scattered wave $F_M(\boldsymbol{r}^*)$ can be non-zero for any value of $\boldsymbol{r}^*$. On the contrary, if the scatterer object is periodic (crystal) we observe a non-zero amplitude only when $\boldsymbol{r}^*$ coincides with a reciprocal lattice point:

$$\boldsymbol{r}^* = \boldsymbol{r}^*_{\mathbf{H}}. \tag{3.25}$$

The function $F_\infty(\boldsymbol{r}^*)$ can be represented by means of a pseudo-lattice: each of its points has the position coinciding with the corresponding point of the reciprocal lattice but has a specific 'weight' $F_M(\mathbf{H})/V$. For a given node the diffraction intensity $I_{\mathbf{H}}$ will be function of the square of its weight.

Let us multiply eqn (3.25) scalarly by $\boldsymbol{a}$, $\boldsymbol{b}$, $\boldsymbol{c}$ and introduce the definition (3.5) of $\boldsymbol{r}^*$: we obtain

$$\boldsymbol{a} \cdot (\boldsymbol{s} - \boldsymbol{s}_0) = h\lambda \qquad \boldsymbol{b} \cdot (\boldsymbol{s} - \boldsymbol{s}_0) = k\lambda \qquad \boldsymbol{c} \cdot (\boldsymbol{s} - \boldsymbol{s}_0) = l\lambda. \tag{3.26}$$

The directions $\boldsymbol{s}$ which satisfy eqns (3.26) are called diffraction directions and relations (3.26) are the **Laue conditions**.

Finiteness of the crystal may be taken into account by introducing the form function $\Phi(\boldsymbol{r})$: $\Phi(\boldsymbol{r}) = 1$ inside the crystal, $\Phi(\boldsymbol{r}) = 0$ outside the crystal. In this case we can write

$$\rho_{cr} = \rho_\infty(\boldsymbol{r})\Phi(\boldsymbol{r})$$

and, because of eqn (3.A.35), the amplitude of the diffracted wave is

$$F(\boldsymbol{r}^*) = \mathrm{T}[\rho_a(\boldsymbol{r})] * [\Phi(\boldsymbol{r})] = F_a(\boldsymbol{r}^*) * D(\boldsymbol{r}^*) \tag{3.27}$$

where

$$D(\boldsymbol{r}^*) = \int_S \Phi(\boldsymbol{r}) \exp(2\pi i \boldsymbol{r}^* \cdot \boldsymbol{r})\, \mathrm{d}\boldsymbol{r} = \int_\Omega \exp(2\pi i \boldsymbol{r}^* \cdot \boldsymbol{r})\, \mathrm{d}\boldsymbol{r}$$

and Ω is the volume of the crystal. Because of eqn (3.A.40) the relation (3.27) becomes

$$\begin{aligned} F(\boldsymbol{r}^*) &= \frac{1}{V} F_{\mathrm{M}}(\mathbf{H}) \sum_{h,k,l=-\infty}^{+\infty} \delta(\boldsymbol{r}^* - \boldsymbol{r}_{\mathbf{H}}^*) * D(\boldsymbol{r}^*) \\ &= \frac{1}{V} F_{\mathrm{M}}(\mathbf{H}) \sum_{h,k,l=-\infty}^{+\infty} D(\boldsymbol{r}^* - \boldsymbol{r}_{\mathbf{H}}^*). \end{aligned} \tag{3.28}$$

If we compare eqns (3.28) and (3.24) we notice that, going from an infinite crystal to a finite one, the point-like function corresponding to each node of the reciprocal lattice is substituted by the distribution function D which is non-zero in a domain whose form and dimensions depend on the form and dimensions of the crystal. The distribution D is identical for all nodes.

For example, let suppose that the crystal is a parallelepiped with faces A_1, A_2, A_3: then

$$D(\boldsymbol{r}^*) = \int_{-A_1/2}^{A_1/2} \int_{-A_2/2}^{A_2/2} \int_{-A_3/2}^{A_3/2} \exp[2\pi i(x^*x + y^*y + z^*z)]\, \mathrm{d}x\, \mathrm{d}y\, \mathrm{d}z.$$

If we integrate this function over separate variables, it becomes, in accordance with Appendix 3.A, p. 174

$$D(\boldsymbol{r}^*) = \frac{\sin(\pi A_1 x^*)}{\pi x^*} \frac{\sin(\pi A_2 y^*)}{\pi y^*} \frac{\sin(\pi A_3 z^*)}{\pi z^*}. \tag{3.29}$$

Each of the factors in eqn (3.29) is studied in Appendix 3.A and shown in Fig. 3.A.1 (p. 174). We deduce:

1. The maximum value of $D(\boldsymbol{r}^*)$ is equal to $A_1A_2A_3$, i.e. to the volume Ω of the crystal;
2. The width of a principal maximum in a certain direction is inversely proportional to the dimension of the crystal in that direction. Thus, because of the finiteness of the crystals each node of the reciprocal lattice is in practice a spatial domain with dimensions equal to A_i^{-1}. In Fig. 3.6 some examples of finite lattices with the corresponding reciprocal lattices are shown.

When we consider the diffraction by a crystal the function $F_{\mathrm{M}}(\mathbf{H})$ bears the name of **structure factor** of vectorial index $\mathbf{H}$ (or indexes h, k, l if we make reference to the components of $\boldsymbol{r}_{\mathbf{H}}^*$) and it is indicated as:

$$F_{\mathbf{H}} = \sum_{j=1}^{N} f_j \exp(2\pi i \boldsymbol{r}_{\mathbf{H}}^* \cdot \boldsymbol{r}_j)$$

where N is the number of atoms in the unit cell. In accordance with

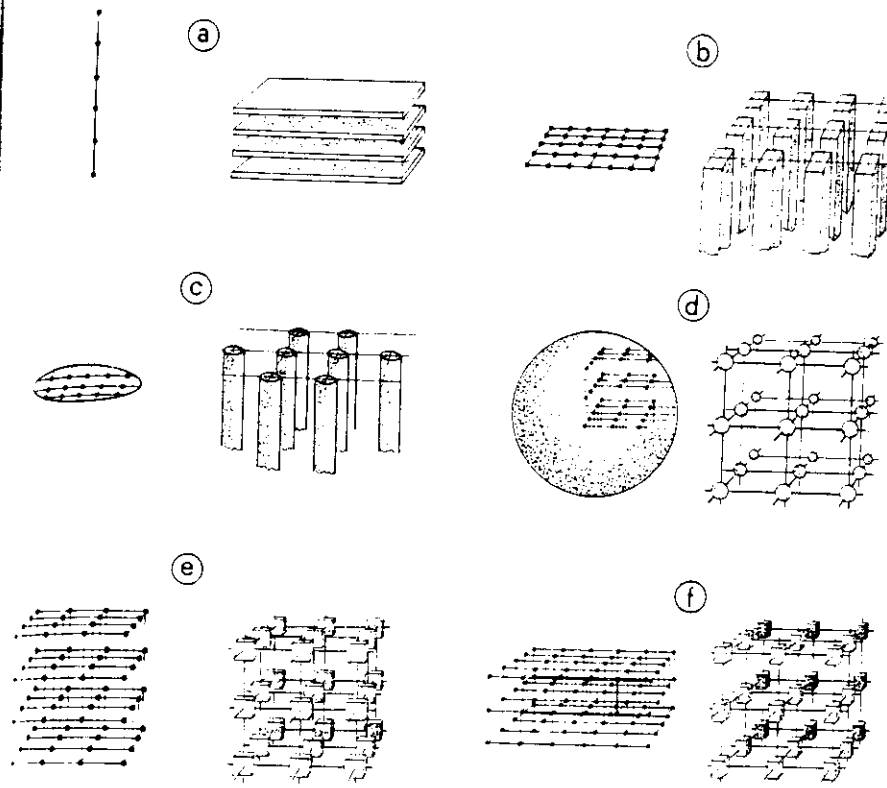

Fig. 3.6. Direct and reciprocal lattices for: (a) a one-dimensional lattice; (b) a two-dimensional lattice in the form of a rectangle; (c) a two-dimensional lattice in the form of a circle; (d) a cubic crystal in the form of a sphere; (e) a cubic crystal in the form of a cube; (f) a crystal in the form of a parallelepiped (from Kitaigorodskii, A. I. (1951). *The theory of crystal structure analysis*, Consultants Bureau, New York).

. 64 we write

$$F_{\mathbf{H}} = \sum_{j=1}^{N} f_j \exp(2\pi \mathrm{i} \bar{\mathbf{H}} \mathbf{X}_j) = A_{\mathbf{H}} + \mathrm{i} B_{\mathbf{H}} \tag{3.30a}$$

here

$$A_{\mathbf{H}} = \sum_{j=1}^{N} f_j \cos 2\pi \bar{\mathbf{H}} \mathbf{X}_j, \qquad B_{\mathbf{H}} = \sum_{j=1}^{N} f_j \sin 2\pi \bar{\mathbf{H}} \mathbf{X}_j. \tag{3.30b}$$

According to the notation introduced in Chapter 2, we have indicated the ector as $r_{\mathbf{H}}^*$ and the transpose matrix of its components with respect to the eciprocal coordinates system as $\bar{\mathbf{H}} = (hkl)$. In the same way r_j is the jth positional vector and the transpose matrix of its components with respect to he direct coordinates system is $\bar{\mathbf{X}}_j = [x_j\ y_j\ z_j]$. In a more explicit form (3.30a) may be written

$$F_{hkl} = \sum_{j=1}^{N} f_j \exp 2\pi \mathrm{i}(hx_j + ky_j + lz_j).$$

In different notation (see Fig. 3.7)

$$F_{\mathbf{H}} = |F_{\mathbf{H}}| \exp(\mathrm{i}\varphi_{\mathbf{H}}) \text{ where } \varphi_{\mathbf{H}} = \arctan(B_{\mathbf{H}}/A_{\mathbf{H}}). \tag{3.31}$$

$\varphi_{\mathbf{H}}$ is the **phase** of the structure factor $F_{\mathbf{H}}$.

If we want to point out in eqn (3.30a) the effect of thermal agitation of he atoms we write, in accordance with p. 149 and Appendix 3.B

$$F_{\mathbf{H}} = \sum_{j=1}^{N} f_{0j} \exp(2\pi \mathrm{i} \bar{\mathbf{H}} \mathbf{X}_j - 8\pi^2 U_j \sin^2 \theta/\lambda^2)$$

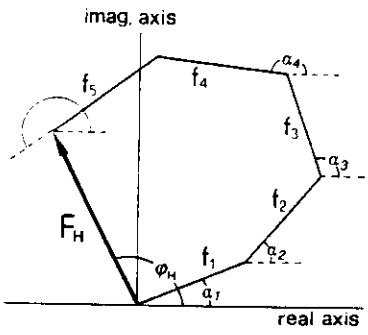

Fig. 3.7. $F_{\mathbf{H}}$ is represented in the Gauss plane for a crystal structure with $N = 5$. It is $\alpha_j = 2\pi \bar{\mathbf{H}} \mathbf{X}_j$.

or

$$F_{\mathbf{H}} = \sum_{j=1}^{N} f_{0j} \exp\left(2\pi i \bar{\mathbf{H}}\mathbf{X}_j - 2\pi^2 \bar{\mathbf{H}}\mathbf{U}_j^* \mathbf{H}\right)$$

depending on the type of the thermal motion (isotropic or anisotropic) of the atoms. f_{0j} is the scattering factor of the jth atom considered at rest. Let us note explicitly that the value of $F_{\mathbf{H}}$, in modulus and phase, depends on the atomic positions i.e. on the crystal structure.

Details of the structure factors calculation from a known structural model are given on pp. 87–8 and Appendix 2.1.

Bragg's law

A qualitatively simple method for obtaining the conditions for diffraction was described in 1912 by W. L. Bragg who considered the diffraction as the consequence of contemporaneous reflections of the X-ray beam by various lattice planes belonging to the same family (physically, from the atoms lying on these planes). Let θ be (see Fig. 3.8) the angle between the primary beam and the family of lattice planes with indices h, k, l (having no integer common factor larger than unity). The difference in 'path' between the waves scattered in D and B is equal to AB + BC = $2d \sin\theta$. If it is multiple of λ then the two waves combine themselves with maximum positive interference:

$$2d_{\mathbf{H}} \sin\theta = n\lambda. \tag{3.32}$$

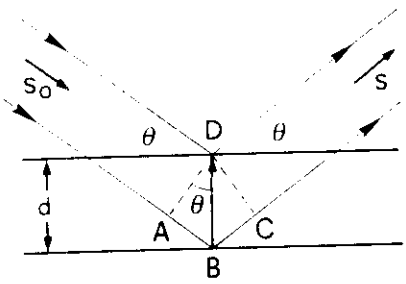

Fig. 3.8. Reflection of X-rays from two lattice planes belonging to the family $\mathbf{H} = (h, k, l)$. d is the interplanar spacing.

Since the X-rays penetrate deeply in the crystal a large number of lattice planes will reflect the primary beam: the reflected waves will interfere destructively if eqn (3.32) is not verified. Equation (3.32) is the **Bragg equation** and the angle for which it is verified is the **Bragg angle**: for $n = 1, 2, \ldots$ we obtain reflections (or diffraction effects) of first order, second order, etc., relative to the same family of lattice planes **H**.

The point of view can be further simplified by observing that the family of fictitious lattice planes with indices $h' = nh$, $k' = nk$, $l' = nl$ has interplanar spacing $d_{\mathbf{H}'} = d_{\mathbf{H}}/n$. Now eqn (3.32) can be written as

$$2(d_{\mathbf{H}}/n) \sin\theta = 2d_{\mathbf{H}'} \sin\theta = \lambda \tag{3.33}$$

where h', k', l' are no longer obliged to have only the unitary factor in common.

In practice, an effect of diffraction of nth order due to a reflection from lattice planes **H** can be interpreted as reflection of first order from the family of fictitious lattice planes $\mathbf{H}' = n\mathbf{H}$.

It is easy to see now that eqn (3.33) is equivalent to eqn (3.25). Indeed, if we consider only the moduli of eqn (3.25) we will have, because of eqn (2.14) and (3.6),

$$r^* = 2 \sin\theta/\lambda = 1/d_{\mathbf{H}}.$$

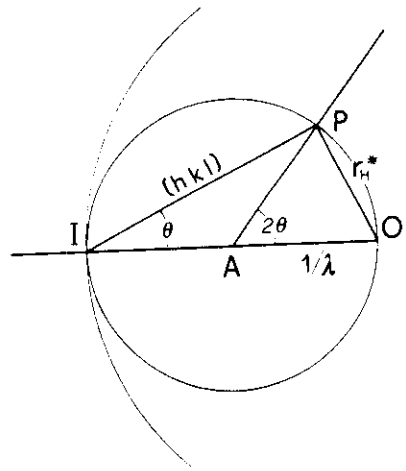

Fig. 3.9. Reflection and limiting spheres.

The reflection and the limiting spheres

Let us outline (see Fig. 3.9) a sphere of radius $1/\lambda$ in such a way that the primary beam passes along the diameter IO. Put the origin of the reciproc

lattice at O. When the vector r_H^* is on the surface of the sphere then the corresponding direct lattice planes will lie parallely to IP and will make an angle θ with the primary beam. The relation

$$OP = r_H^* = 1/d_H = IO \sin\theta = 2\sin\theta/\lambda$$

holds, which coincides with Bragg's equation. Therefore: the necessary and sufficient condition for the Bragg equation to be verified for the family of planes (hkl) is that the lattice point defined by the vector r_H^* lies on the surface of the sphere called the **reflection** or **Ewald sphere**. AP is the direction of diffracted waves (it makes an angle of 2θ with the primary beam): therefore we can suppose that the crystal is at A.

For X-rays and neutrons $\lambda = (0.5–2)$ Å, which is comparable with the dimensions of the unit cell ($\simeq 10$ Å): the sphere then has appreciable curvature with respect to the planes of the reciprocal lattice. If the primary beam is monochromatic and the crystal casually oriented, no point of the reciprocal lattice should be in contact with the surface of the Ewald sphere except the (000) point which represents scattering in the direction of the primary beam. It will be seen in Chapter 4 that the experimental techniques aim to bring as many nodes of the reciprocal lattice as possible into contact with the surface of the reflection sphere.

In electron diffraction $\lambda \simeq 0.05$ Å: therefore the curvature of the Ewald sphere is small with respect to the planes of the reciprocal lattice. A very high number of lattice points can simultaneously be in contact with the surface of the sphere: for instance, all the points belonging to a plane of the reciprocal lattice passing through O.

If $r_H^* > 2/\lambda$ (then $d_H < \lambda/2$) we will not be able to observe the reflection **H**. This condition defines the so-called **limiting sphere**, with centre O and radius $2/\lambda$: only the lattice points inside the limiting sphere will be able to diffract. Vice versa if $\lambda > 2a_{max}$, where a_{max} is the largest period of the unit cell, then the diameter of the Ewald sphere will be smaller than r^*_{min} (the smallest period of the reciprocal lattice). Under these conditions no node could intercept the surface of the reflection sphere. That is the reason why we can never obtain diffraction of visible light (wavelength $\simeq 5000$ Å) from crystals.

The wavelength determines the amount of information available from an experiment. In ideal conditions the wavelength should be short enough to leave out of the limiting sphere only the lattice points with diffraction intensities close to zero due to the decrease of atomic scattering factors.

Diffraction intensities

The theory so far described is called kinematic: basically it calculates interference effects between the elementary waves scattered inside the

volume of the crystal. However, it neglects two important phenomena: when the incident wave propagates inside the crystal its intensity decreases gradually because a part of its energy is transferred to the scattered beam or it is absorbed; the diffracted waves interfere with each other and with the incident beam.

The theory which takes into account all these phenomena and analyses the wave field set up as a whole is called the **dynamic theory of diffraction**. It was initiated by Ewald:[1] later on Laue showed that Ewald's theory is equivalent to analysing the propagation of any electromagnetic field through a medium having a periodically varying complex dielectric constant. The description of the dynamical theory is out of the scope of this book. The reader is referred to specialist books or review articles[2, 3] for exhaustive information. Only a dynamical effect of particular importance for crystal structure analysis, the Renninger effect, will be here described (in Appendix 3.B, p. 191) in any detail. Other dynamical interactions will be described on the basis of the kinematical theory properly modified by Darwin and other authors.

Dynamic effects develop gradually in a crystal: it may be shown that for sufficiently small thicknesses the incident beam is not weakened considerably, the diffracted waves are not yet so strong as to give rise to remarkable interference effects with the incident beam and the effects of absorption are negligible. Under these conditions (theoretically, thicknesses $<10^{-3}$–10^{-4} cm) the kinematic theory is a fairly accurate approximation to dynamic theory. However, in practice, corresponding equations proved to be valid even for crystals having dimensions of several tenths of a millimetre. This is due to the real crystal structures.

A simplified model of real crystal was proposed by Darwin: [4, 5] it can be ideally schematized like a **mosaic** of crystalline blocks with dimensions of about 10^{-3} cm, tilted very slightly to each other for angles of the order of fractions of one minute of arc: each block is separated by faults and cracks from other blocks. The interference between the waves only occurs inside every single block, whose dimensions satisfy the theoretical conditions of applicability of the kinematic theory. Because of the loss of coherence between the waves diffracted from different blocks, the diffracted intensity from the whole crystal is equal to the sum over the intensities diffracted from every single block.

Real crystals, however, differ by ideal ones also because they may contain a large variety of defects, which are convenient to classify into the following groups (see Chapter 9): **transient defects**, having lifetimes measured in microseconds (e.g. phonons, which are elastic waves propagating through the crystal and inducing atomic displacements); **point defects**, which can be missing (called vacancies), interstitial, or vicarious atoms; **line defects**, extending along straight or curved lines (e.g. dislocations); **plane defects**, extending along planes or curved surfaces (e.g. small angle boundaries, stacking faults); **volume defects**, extending throughout small volumes in the crystal (e.g. inclusions, precipitates, voids).

The importance of defects with respect to diffraction intensities depends on their nature and on their density. For example, a single point defect does not produce detectable effects on diffraction maxima but a large number of them, as in the case of order–disorder transitions, strongly affect diffraction. When agglomerated they can form voids or cracks in a crystal

or, clustering along certain planes, they form two-dimensional precipitates. Furthermore, individual dislocations have little effect on diffraction but they may array themselves to form small-angle boundaries separating two relatively perfect regions tilted relative to each other by about one minute of arc (mosaic blocks).

We can therefore expect that any type of defect which disturbs the crystal periodicity by lattice distortion or substitution or shift of atoms from the equilibrium position will produce some effect on diffracted intensities: among others, it will cause a more rapid statistical decrease of diffraction intensities with $\sin\theta/\lambda$. In particular, the lattice distortions cause variations in the unit cell dimensions and therefore modify the form and volume of the reciprocal lattice points (variations of the spacing $d_{\mathbf{H}}$ bring variations in the modulus $r^*_{\mathbf{H}}$, variations in the orientation of the planes $\mathbf{H}$ cause modifications in the orientation of $r^*_{\mathbf{H}}$).

On the basis of these premises it is nonsense to affirm that a crystal is in the 'exact' Bragg position for a given family of lattice planes. Indeed, because of the finite size of the crystal, its mosaic structure, defects, and lattice distortions, etc., each node of the reciprocal lattice will have a finite volume and will be in contact with the surface of the reflection sphere for a finite angle interval. In addition the surface of the reflection sphere itself has in practice to be substituted by a solid domain. Indeed, the incident X-ray beam does have an inevitable divergence and an imperfect monochromaticity. As a consequence (see Fig. 3.11) the spherical surface of radius $1/\lambda$ is replaced by a family of spherical surfaces whose efficiency relative to diffraction depends on the distribution of the intensities as a function of the angle divergence and of the wavelength of the incident beam.

According to the above remarks quantity of practical interest is the integrated intensity and not the maximum intensity of the diffraction peak. Experimental arrangements normally used to measure diffraction intensities change the orientation of the crystal (see Chapter 4) so as to compel reciprocal lattice points to cross progressively the Ewald sphere while continuously recording the intensity of the diffracted beam. Thus the total diffracted energy during a fixed time is measured. Equivalently, the same total energy may be measured by integrating the diffracted intensity over a suitable angular range around the ideal Bragg angle. According to eqns (3.3) and (3.28) the integrated intensity is given by

$$I_{\mathbf{H}} = k_1 k_2 I_0 LPTE\,|F_{\mathbf{H}}|^2 \tag{3.41}$$

where I_0 is the intensity of the incident beam, $k_1 = e^4/(m^2c^4)$ takes into account the universal constants existing in eqn (3.3). $k_2 = \lambda^3\Omega/V^2$ is a

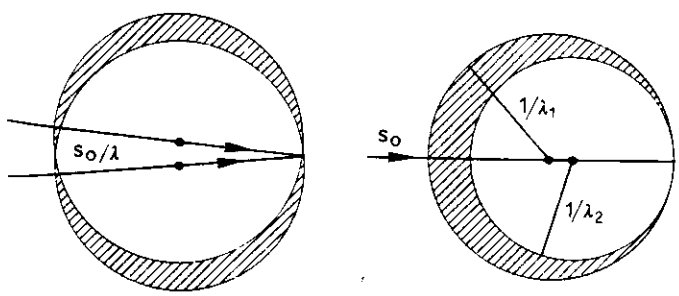

Fig. 3.11. (a) Incident radiation with non-vanishing divergence. (b) Non-monochromatic incident radiation.

constant for a given diffraction experiment (Ω is the volume of the crystal, V is the volume of the unit cell), P is the polarization factor, defined on p. 143, T is the transmission factor and depends on the capacity of the crystal to absorb the X-rays (see Chapter 4, p. 304), L is the Lorentz factor and depends on the diffraction technique (Chapter 4, p. 301). E is the extinction coefficient. It depends on the mosaic structure of the crystal and has two components. The most important one, called **secondary extinction**, takes into account the fact that the lattice planes first encountered by the primary beam will reflect a significant fraction of the primary intensity so that deeper planes receive less primary radiation. That causes a weakening of the diffracted intensity, mainly observable for high-intensity reflections at low $\sin\theta/\lambda$ values in sufficiently perfect crystals. If the mosaic blocks are misoriented (as they usually are) then they do not diffract together and shielding of deeper planes is consequently reduced. Secondary extinction is equivalent to an increase of the linear absorption coefficient: thus it is negligible for sufficiently small crystals. Reflections affected by secondary extinction can be recognized in the final stages of the crystal structure refinement when for some high-intensity reflection $|F_{obs}| < |F_{cal}|$. A method for inclusion of secondary extinction in least-squares methods is recalled in Chapter 2, p. 97.

The second component of the extinction coefficient, called **primary extinction**, takes into account the loss of intensity due to dynamic effects inside every single block. This phenomenon can be understood intuitively by means of Fig. 3.12. At the Bragg angle every incident wave can suffer multiple reflections from different lattice planes: after an odd number of reflections the direction will be the same as the diffracted beam: after an even number of reflections the direction will be the same as the primary beam. Each scattering causes a phase lag of $\lambda/4$. Thus, the unscattered radiation having direction $\mathbf{S}_0$ in Fig. 3.12 is joined by doubly scattered radiation (with much smaller intensity) with a phase lag of π: consequently destructive interference will result. The same consideration holds for waves propagating along the direction of the diffracted beam: the result is that both primary and diffracted beams are weakened because of dynamical effects.

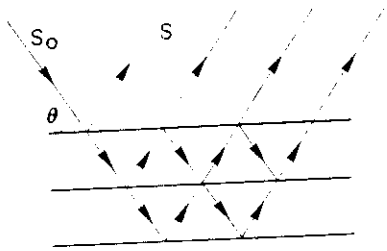

Fig. 3.12. Multiple reflections from a family of lattice planes.

A theory describing the mutual transfer of intensity between incident and diffracted beams was proposed by Zachariasen.[6] If absorption is neglected the intensity I_0 of the beam in the incident direction and the intensity I of the beam in the diffracted direction should be related by:

$$\frac{\delta I_0}{\delta t_0} = -\sigma I_0 + \sigma I$$

$$\frac{\delta I}{\delta t} = \sigma I_0 - \sigma I$$

where t_0 and t are lengths in the direction of the primary and diffracted beams respectively, σ is the diffracted power per unit distance and intensity. The equations have to be solved subject to the boundary conditions: I_0 should be equal to the intensity of the primary beam when $t_0 = 0$ and $I = 0$ when $t = 0$. The sum of the two equations is zero, which is the condition for the conservation of energy. Zachariasen's theory has been modified by other authors:[7–9] the introduction of an extinction correction parameter

least-squares analysis may or may not have, according to circumstances, an appreciable influence on the accuracy of the structural parameters included in the refinement. Indeed prior information on the mosaic structure is not usually available and therefore the corrections which have to be made are not easy to calculate a priori. An experimental (often efficient) way to reduce extinction consists of rapid cooling of the crystal by means of immersion in liquid air: this reduces the dimensions of the mosaic grains.

Anomalous dispersion

It is well known that electrons are bound to the nucleus by forces which depend on the atomic field strength and on the quantum state of the electron. Therefore they have to be considered as oscillators with natural frequencies. If the frequency of the primary beam is near to some of these natural frequencies resonance will take place. The scattering under these conditions is called anomalous and can be analytically expressed by substitution of the atomic scattering factor f_a defined earlier by a complex quantity

$$f = f_a + \Delta f' + if'' = f' + if''.$$

$\Delta f'$ and f'' are called the real and imaginary dispersion corrections. In order to have a simple insight into the problem (a rigorous quantum-mechanical treatment was carried out by Hönl) we recall that the classical differential equation describing the motion of a particle of mass m and charge e in an alternating field intensity $E_{0i} \exp(i\omega t)$ is

$$\frac{d^2x}{dt^2} + g\frac{dx}{dt} + \omega_0^2 x = E_{0i} \exp(i\omega t)$$

where $\omega/2\pi$ is the frequency of the incident wave, ω_0 is the natural angular frequency of the vibrating particle, $g\,dx/dt$ expresses a damping force proportional to the velocity. The steady-state solution of the above equations is

$$x(t) = X_0 \exp(i\omega t)$$

where

$$X_0 = \frac{eE_{0i}/m}{\omega_0^2 - \omega^2 + ig\omega}.$$

If the displacement $x(t)$ is multiplied by e the polarizability moment $[ex(t)]$ of each dipole is obtained; the electrical susceptibility of a collection of Z uncoupled dipoles is then

$$\chi = \frac{ZeX_0}{E_{0i}} = \frac{Ze^2}{m}\frac{1}{\omega_0^2 - \omega^2 + ig\omega}$$

which is a complex function of the frequency of the incident radiation. The electric field produced by the dipole oscillator at a distance $r \gg X_0$ has a magnitude (we neglect the polarization factor and the phase shift due to the travelling in r of the scattered wave) which is $\omega^2/(rc^2)$ times its dipole

moment:

$$E_d = E_{0d}\exp(i\omega t) = \frac{\omega^2 e x(t)}{rc^2} = \frac{\omega^2 e^2}{mrc^2} E_{0i}\frac{\exp(i\omega t)}{\omega_0^2 - \omega^2 + ig\omega}.$$

If the electron is unrestrained and undamped then $g = \omega_0 = 0$ and

$$E_d \equiv (E_d)_{Th} = \frac{-e^2}{mrc^2} E_{0i}\exp(i\omega t)$$
$$= \frac{e^2}{mrc^2} E_{0i}\exp[i(\omega t + \pi)]$$

which well agrees with eqn (3.1) suggested by Thomson: π is the phase lag between the scattered and the incident radiation.

Since $g \ll \omega$, when $\omega \gg \omega_0$ the expression of E_d is not very different from that of a free electron. Therefore Thomson scattering is only applicable when $\omega \gg \omega_0$.

We define now the scattering factor for an electron as the ratio

$$f_e = \frac{E_{0d}}{(E_{0d})_{Th}} = \frac{\omega^2(\omega^2 - \omega_0^2)}{(\omega^2 - \omega_0^2)^2 + g^2\omega^2} + i\frac{g\omega^3}{(\omega^2 - \omega_0^2)^2 + g^2\omega^2}$$
$$= f'_e + if''_e.$$

While the imaginary term is always positive, the real term is negative when $\omega < \omega_0$ and positive when $\omega > \omega_0$. From the quantum-theory point of view, the frequency ω_0 coincides with that of a photon with just sufficient energy to eject the electron from the atom. Such an energy corresponds to the wavelength $\lambda_0 = 2\pi c/\omega_0$ corresponding to the absorption edge. Thus it may be expected that a remarkable deviation from Thomson scattering will arise when the primary beam wavelength is close to an absorption edge of the atom being considered.

An important question is whether $\Delta f'$ and f'' vary with diffraction angle. Existing theoretical treatments suggest changes of some per cent with $\sin\theta/\lambda$ but no rigorous experimental checks have been made so far: therefore in most of the routine applications $\Delta f'$ and f'' are considered to be constant.

For most substances at most X-ray wavelengths from conventional sources dispersion corrections are rather small. Calculated values for CrK_α ($\lambda = 2.291$ Å), CuK_α ($\lambda = 1.542$ Å), and MoK_α ($\lambda = 0.7107$ Å) are listed in the *International tables for x-ray crystallography*, Vol. III. In some special cases ordinary X-ray sources can also generate relevant dispersion effects. For example, holmium has the L_3 absorption edge (=1.5368 Å) very close to CuK_α radiation: in this case the holmium scattering factor is not the same for K_{α_1} and K_{α_2} wavelengths. The following dispersion corrections are calculated:[10]

$CuK_{\alpha_1}(\lambda = 1.5406$ Å): $\quad \Delta f' \simeq -15.41 \quad f'' \simeq 3.70$

$CuK_{\alpha_2}(\lambda = 1.5444$ Å): $\quad \Delta f' \simeq -14.09 \quad f'' \simeq 3.72$

Furthermore, the holmium L_2 absorption edge (=1.3905 Å) is very close to the CuK_β wavelength ($\lambda = 1.3922$ Å), so giving rise to

$$\Delta f' = -11.88, \qquad f' \simeq 8.75.$$

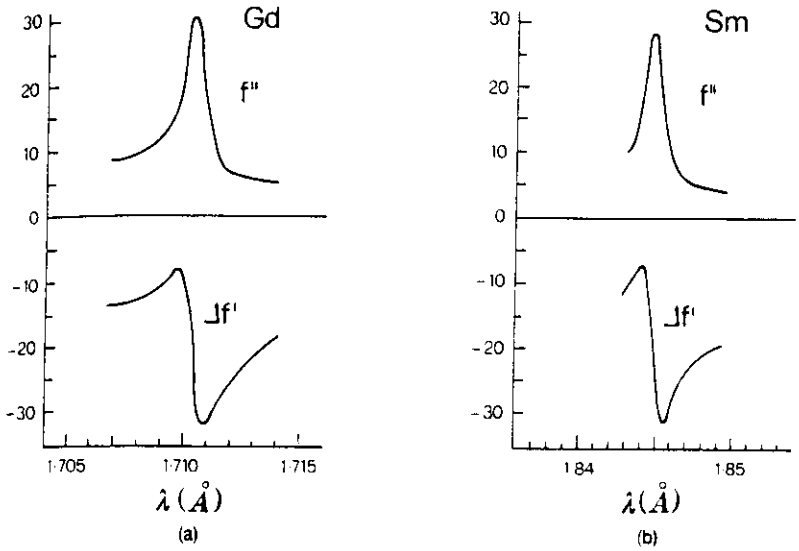

Fig. 3.13. Anomalous scattering terms $\Delta f'$ and f'' for: (a) gadolinium near the L_3 edge; (b) samarium near the L_3 edge.

If synchrotron radiation is used, its intense continuous spectrum may be chosen to high precision in order to provoke exceptionally large anomalous scattering. Very large effects have been measured[11] for rare-earth elements in the trivalent state near L_3 absorption edges (corresponding wavelengths are of crystallographic interest because edges span from 2.26 Å for lanthanum to 1.34 Å for lutetium). In Fig. 3.13 we show the anomalous scattering terms $\Delta f'$ and f'' for gadolinium and samarium near the L_3 absorption edge: spectacular effects as large as ≈30 electrons/atom could be measured.

Since anomalous dispersion may induce substantial variation of the diffracted intensities depending on the wavelength used, anomalous scattering is an important tool for solving crystal structures (see Chapter 8). Several recent works suggest an important role for multiple-wavelength methods: the power of such methods depends on the distances between the working points representing f in the complex plane.[12] As an example, we plot in Figs. 3.14 (a) and (b) the complex scattering factor $\Delta f' + if''$ near the L_3 edge for gadolinium and samarium respectively.

Now we will give only a few elementary ideas about the effects of anomalous dispersion: we postpone the methodological aspects for crystal structure analysis until Chapter 8. Let suppose that a non-centrosymmetric crystal contains N atoms in the unit cell from which P are anomalous scatterers and the remaining $Q = N - P$ atoms are normal scatterers. Then

$$\begin{aligned} F^+ &= F_Q^+ + F_P'^+ + iF_P''^+ = F'^+ + iF_P''^+ \\ F^- &= F_Q^- + F_P'^- + iF_P''^- = F'^- + iF_P''^- \end{aligned} \tag{3.42}$$

where + and − indicate that the magnitudes are calculated for the vectors $\boldsymbol{H}$ and $-\boldsymbol{H}$ respectively. The subscripts P and Q indicate that the structure factors are calculated only with the contribution of P or Q atoms

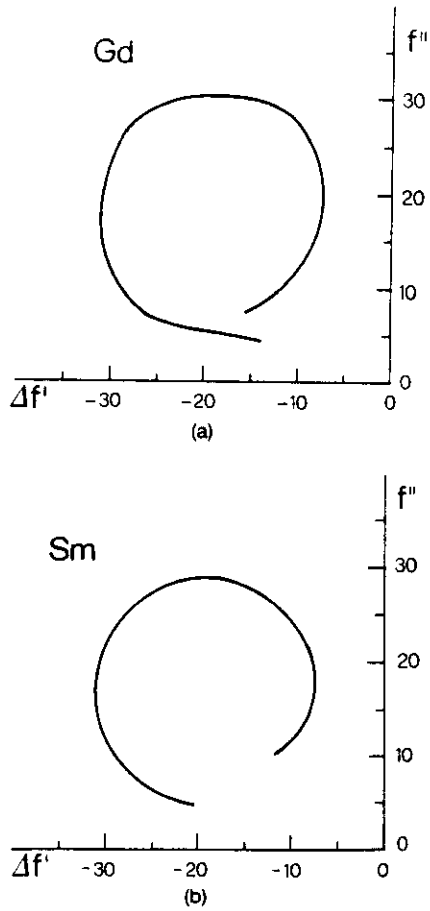

Fig. 3.14. Plot in the complex plane of $\Delta f' + if''$ near the L_3 edge for: (a) gadolinium near the L_3 edge; (b) samarium near the L_3 edge.

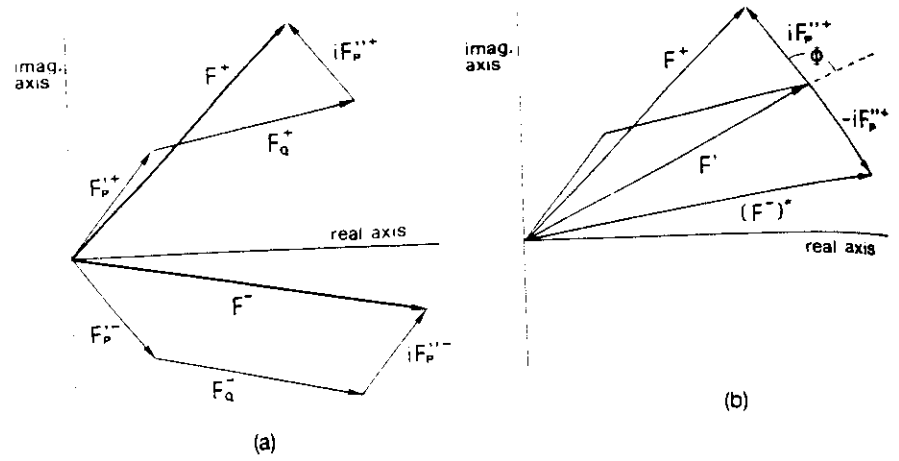

Fig. 3.15. (a) Relation between F_H and F_{-H} when anomalous dispersion is present; (b) relation between F_H and F^*_{-H} when anomalous dispersion is present.

respectively:

$$F'^+_P = \sum_{j=1}^{P} f'_j \exp 2\pi i \tilde{\mathbf{H}}\mathbf{X}_j; \qquad F''^+_P = \sum_{j=1}^{P} f''_j \exp 2\pi i \tilde{\mathbf{H}}\mathbf{X}_j;$$

$$F^+_Q = \sum_{j=P+1}^{P+Q} f_j \exp 2\pi i \tilde{\mathbf{H}}\mathbf{X}_j.$$

The vectors F^+ and F^- are described in Fig. 3.15(a). In Fig. 3.15(b) F^+ and $(F^-)^*$ are shown: the latter is the complex conjugate of F^- and they are symmetric with respect to the real axis:

$$(F^-)^* = F^+_Q + F'^+_P - iF''^+_P = F'^+ - iF''^+_P. \tag{3.43}$$

The difference $\Delta I = |F^+|^2 - |F^-|^2$ is known as the Bijvoet difference[13] and can be easily calculated by means of Fig. 3.15(b):

$$|F^+|^2 = |F'|^2 + |F''_P|^2 + 2|F'||F''_P| \cos\varphi$$
$$|F^-|^2 = |F'|^2 + |F''_P|^2 - 2|F'||F''_P| \cos\varphi$$

from which

$$\Delta I = 4|F'||F''_P| \cos\varphi. \tag{3.44}$$

Furthermore

$$\{|F^+|^2 + |F^-|^2\}/2 = |F'|^2 + |F''_P|^2.$$

In general, as we can see, $|F_H| = |F_{-H}|$ is no longer valid, i.e. the Friedel law is not satisfied in the presence of anomalous dispersion. The value of ΔI depends on the collinearity of F^+_P and F^+_Q. If they are collinear then $|F^+| = |F^-|$: but this happens by mere chance. ΔI is a maximum when F_P and F_Q are approximately at the right angles.

The Friedel law is satisfied if: the structure is centrosymmetric—in this case $|F^+|$ and $|F^-|$ are always equal; the reflection is centrosymmetric even if the structure is non-centrosymmetric; the crystal is constituted of only one chemical element which is the anomalous scatterer.

As a last observation it should be mentioned that besides X-ray, neutron and gamma-ray anomalous dispersion are also very useful in crystal structure analysis. Neutron anomalous dispersion techniques employ

nuclear isotopes with resonances in the range of thermal-neutron energies (see p. 198 for further details).

Gamma-rays are elastically scattered by the electrons of the atoms in the crystal. An elastic resonant scattering by the nucleus (Mössbauer effect) also occurs—the transition involves energies comparable with those employed in conventional X-ray diffraction. Since both the processes are coherent, scattering by resonant nuclei (there are no other nuclear scattering contributions) and by electrons can occur simultaneously and interfere with each other.

An ideal nucleus for gamma-ray resonance is ^{57}Fe; its 14.4 keV resonance corresponds to a wavelength of 0.86 Å. A widely used experimental set-up includes a radioactive source which emits the 14.4 keV radiation in the decay of the parent isotope ^{57}Co. This produces a resonance effect in ^{57}Fe (this atom may naturally be present in the crystal or implanted by techniques such as those used for isomorphous replacement) which is superimposed on the various Bragg reflections upon the gamma radiation elastically scattered by all the atoms in the crystal, iron atoms included. Since ^{57}Fe has a natural abundance of about 2.2 per cent, isotopic enrichment techniques must be applied in order to provide a sufficiently large resonant scattering.

The frequency of the incident radiation may be modified by moving the radiation source, at low velocity (some mm s^{-1}), towards or away from the crystal (linear Doppler effect).

The anomalous scattering amplitudes increase dramatically in going from X-ray to neutron to gamma-ray. Conversely, the intensities of the radiation sources decrease dramatically. This is the most severe drawback for the use of gamma rays: relatively large signals are produced by relatively very weak radiation sources.

The Fourier synthesis and the phase problem

If the structure factors are known in modulus and phase the atomic positions are unequivocally determinable. Indeed, according to eqn (3.A.16) the electron density is the inverse Fourier transform of $F(\boldsymbol{r}^*)$:

$$\begin{aligned}\rho(\boldsymbol{r}) &= \int_{S^*} F(\boldsymbol{r}^*) \exp(-2\pi i \boldsymbol{r}^* \cdot \boldsymbol{r})\, d\boldsymbol{r}^* \\ &= \frac{1}{V} \sum_{h,k,l=-\infty}^{+\infty} F_{hkl} \exp[-2\pi i(hx + ky + lz)].\end{aligned} \tag{3.45}$$

$\dot{\mathbf{X}} \equiv [x, y, z]$ are the fractional coordinates of the point defined by the vector $\boldsymbol{r}$. The atomic positions will correspond to the maxima of $\rho(\boldsymbol{r})$.

If in eqn (3.45) we sum up the contributions of $\boldsymbol{H}$ and $-\boldsymbol{H}$ we will have

$$\begin{aligned}&F_{\mathbf{H}} \exp(-2\pi i \bar{\mathbf{H}}\mathbf{X}) + F_{-\mathbf{H}} \exp(2\pi i \bar{\mathbf{H}}\mathbf{X}) \\ &\quad = (A_{\mathbf{H}} + iB_{\mathbf{H}}) \exp(-2\pi i \bar{\mathbf{H}}\mathbf{X}) + (A_{\mathbf{H}} - iB_{\mathbf{H}}) \exp(2\pi i \bar{\mathbf{H}}\mathbf{X}) \\ &\quad = 2[A_{\mathbf{H}} \cos 2\pi \bar{\mathbf{H}}\mathbf{X} + B_{\mathbf{H}} \sin 2\pi \bar{\mathbf{H}}\mathbf{X}]\end{aligned}$$

from which

$$\rho(\boldsymbol{r}) = \frac{2}{V} \sum_{h=0}^{+\infty} \sum_{k=-\infty}^{+\infty} \sum_{l=-\infty}^{+\infty} \times [A_{hkl} \cos 2\pi(hx + ky + lz) + B_{hkl} \sin 2\pi(hx + ky + lz)] \quad (3.46)$$

is obtained. The right-hand side of (3.46) is explicitly real and is a sum over a half of the available reflections.

The mathematical operation represented by the synthesis (3.46) can be interpreted as the second step in the process of formation of an image in optics. The first step consists of the scattering of the incident radiation which gives rise to the diffracted rays with amplitudes $F_{\mathbf{H}}$. In the second step the diffracted beams are focused by means of lenses, and by interfering with each other they create the image of the object. There are no physical focusing lenses for X-rays but they can be substituted by a mathematical lens (exactly, by Fourier synthesis (3.46)).

Because of the decrease of the atomic scattering factors the diffraction intensities (and consequently $|F_{\mathbf{H}}|$) weaken 'on average' with the increase of $\sin\theta/\lambda$ and can be considered zero for values above a given $(\sin\theta/\lambda)_{max} = 1/(2d_{min})$. Since the reflections at high values of $\sin\theta/\lambda$ give the fine details of the structure (small variations of the atomic coordinates can produce big changes in high-angle structure factors) the quantity d_{min} is adopted as a measure of the natural resolution of the diffraction experiment. d_{min} depends on different factors such as: the chemical composition of the crystal (heavy atoms are good scatterers even at high values of $\sin\theta/\lambda$), the chemical stability under the experimental conditions of temperature and pressure, the radiation used (the resolution improves when we pass from electrons to X-rays and neutrons), the temperature of the experiment. Roughly speaking, for X-rays d_{min} can reach the limit of 0.5 Å in inorganic crystals, 0.7–1.5 Å in organic crystals, and 1.0–3 Å in protein crystals.

Because of the limit of natural resolution or of an artificially introduced limit (for instance in order to save time and calculations) the electron density function will be affected by errors of termination of series. The effect can be mathematically evaluated by calculating the function $\rho'(\boldsymbol{r})$ available via the function

$$F'(\boldsymbol{r}^*) = F(\boldsymbol{r}^*)\Phi(\boldsymbol{r}^*).$$

$\Phi(\boldsymbol{r}^*)$ is the form function: $\Phi(\boldsymbol{r}^*) = 1$ inside the available reflection sphere, $\Phi(\boldsymbol{r}^*) = 0$ outside this sphere. According to eqn (3.A.35) we have

$$\rho'(\boldsymbol{r}) = \mathrm{T}[F'(\boldsymbol{r}^*)] = \rho(\boldsymbol{r}) * \mathrm{T}[\Phi(\boldsymbol{r}^*)]. \quad (3.47)$$

If $\boldsymbol{r}^*$ is the radius of the available reflection sphere, according to Appendix 3.A, p. 181, $\mathrm{T}[\Phi(\boldsymbol{r}^*)]$ is a function with a maximum at $\boldsymbol{r} = 0$ and the subsidiary maxima of weight decreasing with $1/r^2$. The effect of the convolution (3.47) is qualitatively represented in Fig. 3.16. In particular, even if $\rho(\boldsymbol{r})$ is positive everywhere, $\rho'(\boldsymbol{r})$ can be negative in more or less extended regions: the atomic peaks can be broad and surrounded by a series of negative and positive ripples of gradually decreasing amplitude.

The number of reflections used in practice in eqn (3.46) varies from several tens or hundreds, for unit cells of small dimensions, to several tens of thousands for macromolecules.

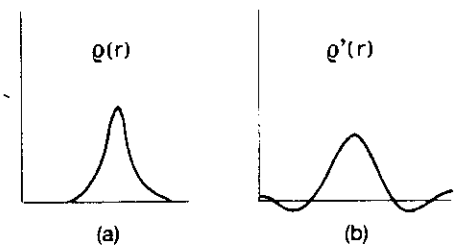

Fig. 3.16. (a) Electron density $\rho(\boldsymbol{r})$; (b) electron density obtained via a Fourier synthesis with series termination errors.

In order to reveal the atomic positions, $\rho'(r)$ is sampled upon a three-dimensional grid whose spacings along each of the unit-cell axes have to be fixed with some care. If the grid is too coarse the interpolation between grid points to find the maximum of the electron density may be uncertain, if the grid is too fine a great deal of computing may be unnecessary. In absence of symmetry, at a resolution d_{min} there are

$$N_r = \frac{4\pi}{3d_{min}^3 V^*} = \frac{4\pi V}{3d_{min}^3}$$

measurable (only $N_r/2$ independent) reflections and the number of grid points is $N_p \simeq V/\Delta^3$ where Δ is the grid spacing (say 0.2–0.4 Å in the three directions). In practical cases N_r and N_p are rather large: for instance, for $V = 1000$ Å^3, $d_{min} = 0.8$ Å, $\Delta = 0.25$ Å, we have $N_r \simeq 8180$ and $N_p \simeq 64\,000$.

If symmetry is present the amount of calculation is smaller. The number of independent reflections to be measured is roughly $N_r/(\tau m)$ where τ is the centring order of the cell and m the multiplicity factor of the Laue class (this is not strictly exact as the multiplicity factor refers to general reflections of type (hkl) and may be different and less than m for certain zones of reflections). Furthermore, it will be sufficient to sample ρ upon the grid points lying inside the asymmetric unit for reconstructing the whole content of the cell.

For instance, let P2/m be the space group with $a = 7.8$ Å, $b = 16.2$ Å and $c = 8.1$ Å and $\beta = 93^0$. If we divide a and c into 33 and b into 66 intervals the grid spacing will have a sufficient and almost identical resolution in all three directions. The number of grid points lying inside the asymmetric unit (1/4 of the unit cell) is now $33 \times 33 \times 17 = 18\,513$.

Very often the volume of the unit cell is much larger than 10^3 Å^3 ($V > 10^6$ Å^3 is not infrequent for macromolecules). Thus even with the use of high-speed computers, the calculation of ρ is a fairly arduous task involving time-consuming procedures. Different algorithms are used to make calculations faster. The most convenient are the Beevers–Lipson technique and the fast Fourier transform algorithm by Cooley and Tookey (see Chapter 2, pp. 88–90, and Appendix 2.I).

Unfortunately, it is not possible to apply eqn (3.47) only on the basis of information obtained directly from X-ray diffraction. Indeed, according to eqn (3.41), only the moduli $|F_H|$ can be obtained from diffraction intensities because the corresponding phase information is lost. This is the so-called **crystallographic phase problem**: how to identify the atomic positions starting only from the moduli $|F_H|$. A general solution to the problem has not been found, but there are methods we can successfully apply (see Chapters 5 and 8).

PROPERTIES OF SYNCHROTRON RADIATION	ADVANTAGES IN CRYSTALLOGRAPHY
HIGH INTENSITY	RAPID DATA COLLECTION POSSIBLE SMALL CRYSTALS CAN BE USED WEAK, HIGH RESOLUTION DATA CAN BE MEASURED
TUNEABLE WAVELENGTH	DATA CAN BE COLLECTED NEAR ABSORPTION EDGES OF HEAVY ATOMS HIGH RESOLUTION DATA CAN BE COLLECTED ON FILM OF MANAGEABLE SIZE
WHITE RADIATION	LAUE METHOD VERY RAPID DATA COLLECTION KINETIC MEASUREMENTS POSSIBLE
HIGH COLLIMATION	WELL DEFINED REFLECTIONS HIGHER RESOLUTION DATA OBTAINABLE
PULSED TIME STRUCTURE	USE IN KINETIC MEASUREMENTS
POLARIZATION OF RADIATION	NOT YET USED IN CRYSTALLOGRAPHY